$$\begin{pmatrix} \dot{\theta} \\ \dot{\omega}_0 \\ \dot{\gamma} \\ \dot{\omega}_R \end{pmatrix} = \begin{bmatrix} 0 & E & 0 & 0 \\ 0 & 0 & \alpha^{-1}A_{12}A_{22}^{-1}K & \alpha^{-1}A_{12}A_{22}^{-1}B \\ 0 & 0 & 0 & E \\ 0 & 0 & -A_{22}^{-1}(E+A_{21}\alpha^{-1}A_{12}A_{22}^{-1})K & -A_{22}^{-1}(E+A_{21}\alpha^{-1}A_{12}A_{22}^{-1})B \end{bmatrix} \begin{pmatrix} \theta \\ \omega_0 \\ \gamma \\ \omega_R \end{pmatrix} + \begin{bmatrix} 0 \\ \alpha^{-1}\bar{L}_0 - \alpha^{-1}A_{12}A_{22}^{-1}\bar{L}_R \\ 0 \\ A_{22}^{-1}(E+A_{21}\alpha^{-1}A_{12}A_{22}^{-1})\bar{L}_R - A_{22}^{-1}A_{21}\alpha^{-1}\bar{L}_0 \end{bmatrix} \tag{1}$$

where

$$\alpha = [A_{11} - A_{12}A_{22}^{-1}A_{21}] \tag{2}$$

Stochastic Controller for Multihinged Rigid-Body Spacecraft

In this section, a stochastic controller based on the dynamical model presented above is given. The form of the stochastic controller appropriate for a linear problem subject to a quadratic cost functional is retained; however, the form of the control function for this special case is passed through desirable nonlinearities peculiar to attitude control before being applied to the plant (see Fig. 1).

In this analysis, the suboptimal vector function u_0 for the base body is obtained by

1) Generating the actuating signal $\bar{u}$ used to fire the thrusters located on the base body according to (note that $\bar{u}$ retains the structure of the optimal u^* for a linear problem but the control gains are obviously not based on the linear formulation)

$$\bar{u} = C_\theta \hat{\theta} + C_{\omega_0}\hat{\omega}_0 + C_\gamma \hat{\gamma} + C_{\omega_R}\hat{\omega}_R \tag{3}$$

2) Passing the function $\bar{u}$ through a vector deadzone function to obtain the applied moment M_0 and the associated applied thrust F_0 acting on the base body; this contribution to u_0 is given by

$$M_0 = -\left[\sum_{i=1}^{3} |M_{0_i}|\, b_i b_i^T\right] DEZ\, \bar{u} \tag{4}$$

3) Generating the terms $\bar{L}_{00}$, L_{0R}, and L_{R0}. The vector control function u_0 is given by

$$u_0 = \alpha^{-1}\left[-\sum_{i=1}^{3} |M_{0_i}|\, b_i b_i^T\right] DEZ\, \bar{u} + \alpha^{-1}\bar{L}_{00} + \alpha^{-1}L_{0R} - \alpha^{-1}A_{12}A_{22}^{-1}(L_{R0}+L_{RR}) \tag{5}$$

Correspondingly, the vector control function for the remaining $n-1$ bodies is given by

$$u_R = -A_{22}^{-1}A_{21}u_0 + A_{22}^{-1}(L_{R0}+L_{RR}) \tag{6}$$

Note that the time-varying functions $\bar{L}_{00}$, L_{0R}, L_{R0}, and L_{RR} are based on $\hat{\gamma}$. The control gains C_θ, C_{ω_0}, C_γ, C_{ω_R} are, of course, selected so that the pointing requirements are met.

Description and Uses of Suboptimal Stochastic Controller

From Fig. 1 it is seen that the stochastic controller consists of a Kalman filter adjoined to the generators of u_0 and u_R. The measurement vector z, in this paper, consists of the sensed attitude angles of the base body. The estimated state $\hat{x}$ consisting of $\hat{\theta}$, $\hat{\omega}_0$, $\hat{\gamma}$, $\hat{\omega}_R$ is used to generate the actuating signal $\bar{u}$ which fires the thrusters located on the base body. In essence, the applied moment M_0 tends to null a weighted combination of the attitude and angular velocity of the base body and the relative motion of the remaining $n-1$ bodies. Note that, if it is not desirable to null a specific relative motion γ_k and its associated rate $\dot{\gamma}_k$, then the appropriate components of the control gain matrices C_γ and C_{ω_R} are zero. Note, too, that the system matrices A_{11}, A_{22}, A_{12}, A_{21}, α are constant. The Kalman gain matrices $\bar{K}_\theta$, $\bar{K}_{\omega_0}$, $\bar{K}_{\omega_R}$, $\bar{K}_\gamma$ and the control gain matrices C_θ, C_{ω_0}, C_{ω_R}, C_γ can be approximated by piecewise constant functions, if it is so desired.

This stochastic controller will be used to study the effects of interactions of an articulated science platform (undergoing small-angle slews) on the base body motion, and to study the effects of interactions of booms (undergoing small oscillations) on thrust vector control performance. Specifically, this controller will be used to analyze the Mariner Jupiter Saturn (MJS '77) spacecraft in the cruise, the thrust vector control, and the articulation control modes. The MJS '77 stringent accuracy requirements and settling times associated with the articulated science platform dictates that an elaborate dynamical model be used and that disturbances and sensor noise be properly accounted for. It is planned that the computational aspects and simulation results obtained from this formulation will be published in the near future.

References

[1] Hooker, W. W. and Margulies, G., "The Dynamical Attitude Equations for an n-Body Satellite," *Journal of the Astronautical Sciences*, Vol. XII, No. 4, Winter 1965, pp. 123–128.

[2] Hooker, W. W., "A Set of r Dynamical Attitude Equations for an Arbitrary n-Body Satellite Having r Rotational Degrees of Freedom," *AIAA Journal*, Vol. 8, No. 7, July 1970, pp. 1205–1207.

[3] Likins, P. W., "Dynamical Analysis of a System of Hinge-Connected Rigid Bodies with Nonrigid Appendages," to be published.

[4] Likins, P. W. and Fleischer, G. E., "Large-Deformation Modal Coordinates for Nonrigid Vehicle Dynamics," TR 32-1565, Nov. 1, 1972, Jet Propulsion Lab., Pasadena, Calif.

[5] Larson, V., "Dynamical Models for a Spacecraft Idealized as a Set of Multi-Hinged Rigid Bodies," TM 33-613, May 1, 1973, Jet Propulsion Lab., Pasadena, Calif.

[6] Larson, V., "State Equations for an n-Body Spacecraft," to be published in *Journal of Astronautical Sciences*.

[7] Special Issue on Linear-Quadratic Gaussian Problem, *IEEE Transactions on Automatic Control*, Vol. AC-16, No. 6, Dec. 1971.

Optimal Payload Ascent Trajectories of Winged Vehicles

JAMES A. MARTIN*

NASA Langley Research Center, Hampton, Va.

Nomenclature

$\bar{m}$ = mass at burnout normalized by W

$\bar{q}\bar{\alpha}$ = product of dynamic pressure and angle of attack normalized by the reference condition value of 33 516 N-deg/m^2 (700 lb-deg/ft^2) (see Fig. 2)

r = recovery resizing factor, vehicle inert mass growth per unit mass of subsystem growth

$\underline{W}$ = wing mass at the reference condition, 5149 kg (11,352 lb)

$\overline{\Delta W}$ = change in wing mass normalized by W

Received May 1, 1974; revision received August 13, 1974.

Index categories: Launch Vehicle and Missile Trajectories; Launch Vehicle and Missile Structural Design.

* Aerospace Engineer, Space Systems Division. Associate Member AIAA.

Introduction

THE launch vehicles used in the 1960's have usually followed essentially zero-lift ascent trajectories because airloads are minimized and the typically cylindrical shape provides little lifting capability. The advent of winged, reusable launch vehicle systems such as the current NASA space shuttle design alters this situation. Previous trajectory analyses have illustrated the potential for improvement in burnout mass obtainable through lifting ascent with optimized pitch histories,[1,2] but the corresponding change in wing mass was not considered. In this Note, the benefit of lifting ascent including the penalties associated with increased wing mass due to increased aerodynamic loading are presented.

Vehicle and Procedure

The vehicle analyzed, shown in Fig. 1, consisted of an orbiter, an expendable liquid fuel tank, and two solid rocket motors. The orbiter was an in-house Langley Research Center design with some internal fuel, with shape and aerodynamics as described in Refs. 3 and 4. The solid-rocket boosters and the orbiter main engines were ignited at lift-off (parallel burn) and the solid-rocket boosters and external tank were staged when empty. The internal fuel provided the final acceleration to achieve orbital insertion. The propulsion elements were constant for the study; variations in the orbiter injected mass were reflected in the liftoff mass. The mass properties used in the study were as follows: orbiter, 18–19W; internal fuel, 2W; external fuel, 197W; solid-rocket boosters, 112W; lift-off mass, 329–330W.

Figure 2 shows the effect of $\overline{q\alpha}$ on wing mass. The data shown were provided by Grumman Aerospace Corp., Bethpage, N.Y., under contract to Langley Research Center. The calculations of the wing mass were based on maximum loading conditions, and the conditions considered included all wind gusts given in Ref. 5 added vectorially at points along no-wind trajectories. The reference condition ($\overline{q\alpha} = 1$) was originally selected to equalize headwind and tailwind gust effects and therefore minimize wing mass, and the reference wing and orbiter masses were calculated for this condition. Further investigation indicated that $\overline{q\alpha} = 1$ did not minimize wing mass, but the reference condition was not changed. The data points were connected by linear segments because the design loading condition varied for different values of $\overline{q\alpha}$ examined, and slope discontinuities were therefore expected. For $\overline{q\alpha}$ of 3 to 4, the slope changes little between segments (see Fig. 2). The range of $\overline{q\alpha}$ of 3 to 4 is of primary interest for maximum burnout mass. This is indicated on Fig. 3 which will be discussed later.

The trajectories were integrated with the optimization program POST.[6] This program numerically integrates point-mass trajectories and varies specified control parameters to satisfy constraints and maximize a desired variable. The trajectories were assumed to consist of several segments over which the pitch rates were constant. The effect of this assumption, compared to

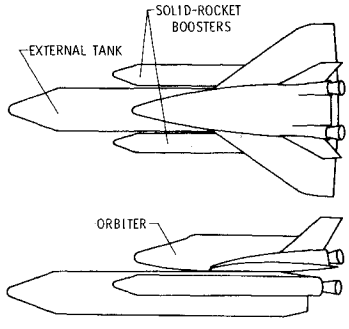

Fig. 1 Sketch of typical two-stage launch vehicle with parallel-burning solid-rocket boosters and external fuel tank.

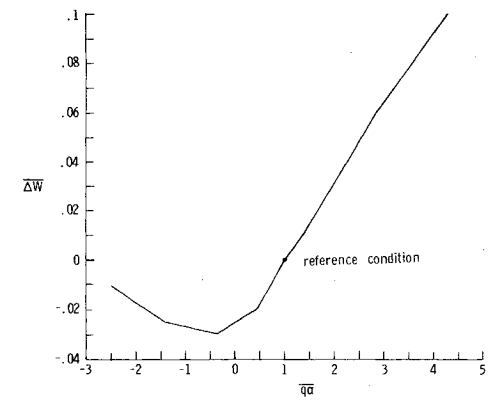

Fig. 2 Effect of trajectory constraint ($\overline{q\alpha}$) on wing mass.

continuously-varying pitch rates, has been found to be insignificant. The pitch angles at the ends of these segments were varied to maximize the burnout mass subject to the constraints of achieving the desired insertion orbit (50 naut mile perigee and 100 naut mile apogee), the dynamic pressure limit of 31, 122 n/m^2 (650 lb/ft^2), and the limit on the product of dynamic pressure and angle-of-attack, $\overline{q\alpha}$. Trajectories were optimized for various values of $\overline{q\alpha}$ to establish the variation of injected mass.

Results and Conclusions

The results of the tradeoff are shown in Fig. 3; the parameters plotted differ from the payload by a constant. The top curve ($r = 0$) shows that the total vehicle injected mass $\bar{m}$ increases with $\overline{q\alpha}$ at a decreasing rate. The second curve represents the effect on the payload if the increase in wing mass alone is considered; an optimum occurs at $\overline{q\alpha}$ about 3.9. In the lowest curve allowance has been made for the increase in wing mass plus the increase in other elements when the vehicle is resized to carry the increased wing structure. The recovery resizing factor was assumed to be 1.6, which is representative of the results for numerous design studies for winged reusable vehicles such as Refs. 7 and 8. The lowest curve is considered to be the most realistic basis on which to select the optimum value of $\overline{q\alpha}$. The total benefit from lifting trajectories is not shown because no trajectories were calculated that had $\overline{q\alpha} = 0$ which would give a ballistic trajectory, but the range investigated shows that the payload can be improved significantly. Increasing $\overline{q\alpha}$ from 1.5 to 3.6 increases $\bar{m} - 1.6\,\bar{W}$ and therefore the payload about 0.45W, or 2300 kg (5100 lb). This is 13% of the design payload to 100 naut mile polar orbit at $\overline{q\alpha} = 3.6$, which was 18,000 kg (40,000 lb). Lifting ascent therefore provides a

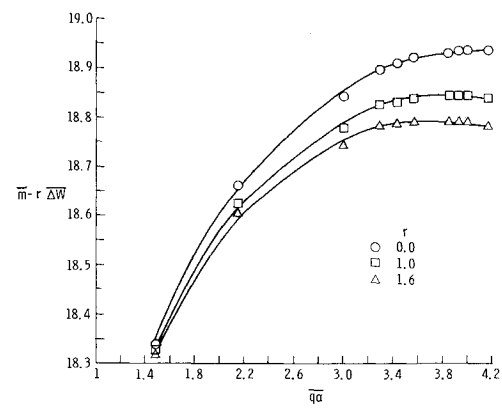

Fig. 3 Effect of trajectory constraint on payload with corrections for wing mass.

payload delivery increase even when structural mass penalties are accounted for.

References

[1] Elliot, J. R. and Rau, T. R., "Optimum Use of the Earth Atmosphere for Shuttle Ascent," *Deutschen Gesellschaft für Luft- und Raumfahrt Journal for Raumfahrtforschung* Band 16, Heft 2, March–April 1972.

[2] Elliot, J. R. and Rau, T. R., "Optimal Payload Trajectory Characteristics for Winged Booster Vehicles." *Journal of Spacecraft and Rockets,* Vol. 5, No. 2, Feb. 1968, pp. 218–220. Huntsville, Ala., 1967.

[3] Ware, G. M. and Spencer, B., Jr., "Low Subsonic Aerodynamics Characteristics of a Shuttle Orbiter Configuration Designed for Reduced Length," TMX-2712, 1973, NASA.

[4] Stone, H. W., "Supersonic and Hypersonic Aerodynamic Characteristics of two Shuttle-Orbiter Configuration Designed for Reduced Length" TMX-71956, April 1974, NASA.

[5] Daniels, G. E., Terrestrial Environment (Climatic) Criterial Guidelines for Use in Aerospace Vehicle Development, 1973 Revision, TMX-64757, July, 1973, NASA.

[6] Brauer, G. L., Cornick, D. E., Steinhoff, R. J., and Stevenson, R., Program to Optimize Simulated Trajectories (POST), Rept. MCR–73–206, Oct. 1973, Martin Marietta Corp., Denver, Colo.

[7] "Phase B Final Report," Rept. SD 71–114–2, March 1971, North American Rockwell, Downey, Calif.

[8] "Alternate Space Shuttle Concepts Study Final Report," Rept. B35–43RP–12, July 1971, Grumman Aerospace Corp., Bethpage, N.Y.

Design Considerations for Space Chamber Cryopanels

K. SRINIVASAN,* V. SESHAGIRI RAO,† AND M. V. KRISHNA MURTHY‡

Indian Institute of Technology, Madras, India

Nomenclature

A = cross-sectional area of fin tube, cm^2
a = radius of the test specimen, cm
d_1 = inner diameter of the fin tube, cm
d_2 = outer diameter of the fin tube, cm
F_{12} = shape factor
f = factor defined in Eq. (20)
K = thermal conductivity, w/cm-K
L = length of the fin, cm
L_1 = length of the fin to the point of tangent, cm
n = number of tubes per meter length
R = radius of the cryopanel, cm
t = thickness of rectangular fin, cm
t_1 = tip thickness of trapezoidal fin, cm
t_2 = base thickness of trapezoidal fin, cm
T = temperature, K
T_1 = temperature of test specimen, K
X = defined in Eq. (12), cm^2
Z = coordinate axis, cm
θ, ϕ = angles, °
σ = Stefan's constant, w/cm^2-K^4
ε = emissivity

Received May 29, 1974; revision received July 1, 1974.

Index categories: Spacecraft Ground Testing and Simulation (Including Loads); Thermal Modeling and Experimental Thermal Simulation.

* Research Scholar, Refrigeration and Airconditioning Laboratory, Department of Mechanical Engineering.

† Lecturer, Refrigeration and Airconditioning Laboratory, Department of Mechanical Engineering.

‡ Assistant Professor, Refrigeration and Airconditioning Laboratory, Department of Mechanical Engineering.

Introduction

LIQUID nitrogen cooled cryopanels are used in space simulation chambers for simulating heat sink effects of the outer space. The design criteria for cryopanels are: a) optical tightness, b) provision of high conductance paths for evacuating the test volume, and c) minimum cooldown mass. Many fin tube configurations were used in the past for meeting these criteria.[1] The selection of a particular fin configuration has been mainly arbitrary. In this analysis the heat-transfer characteristics of cryopanel sections are studied for a given temperature drop, base and tip thicknesses of fin. A method of calculating other parameters of the cryopanel geometry is presented. A selection criteria for fin configuration is evolved.

Physical Model

The physical models for the fin analysis and geometry parameters are shown in Figs. 1 and 2, respectively. It is assumed that the test specimen is spherical and its diameter is equal to one half the diameter of cryopanel, which is assumed to be cylindrical. The maximum temperature at any point on the fin is assumed to be 100 K. The spacecraft and cryopanel emissivities are taken as 0.2 and 0.9, respectively. Radiant exchange between the fin and its base or other parts of the cryopanel is neglected. The temperature perpendicular to the fin length is lumped. Constant thermal properties of the fin material are assumed. The maximum heat flux incident on the test specimen is taken as 1.4 solar constants.

Location of Fin for Maximum Heat Transfer

In radial and tangential fin cases, the base heat flux is the same for a given configuration. The heat transfer area available is proportional to OX in a radial fin and to OY in

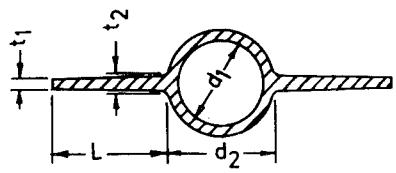

Fig. 1a Radial fin tube.

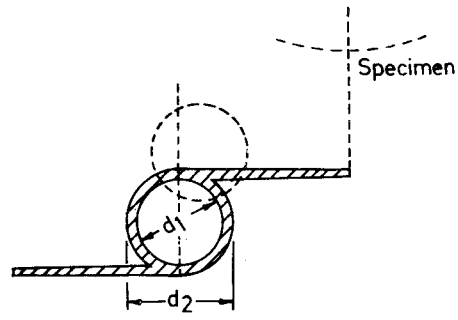

Fig. 1b Tangential fin tube.

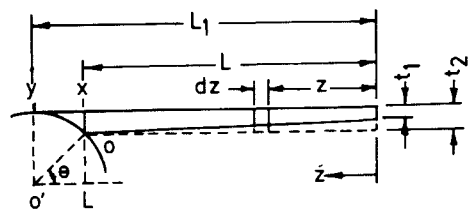

Fig. 1c Physical model for heat-transfer analysis.